



**HAL**  
open science

## First experiments with Cs doped Mo as surface converter for negative hydrogen ion sources

L. Schiesko, Gilles Cartry, C. Hopf, T. Höschen, G. Meisl, O. Encke, B. Heinemann, K. Achkasov, P. Amsalem, U. Fantz

### ► To cite this version:

L. Schiesko, Gilles Cartry, C. Hopf, T. Höschen, G. Meisl, et al.. First experiments with Cs doped Mo as surface converter for negative hydrogen ion sources. *Journal of Applied Physics*, 2015, 118 (7), pp.073303. 10.1063/1.4928861 . hal-03617714

**HAL Id: hal-03617714**

**<https://amu.hal.science/hal-03617714>**

Submitted on 23 Mar 2022

**HAL** is a multi-disciplinary open access archive for the deposit and dissemination of scientific research documents, whether they are published or not. The documents may come from teaching and research institutions in France or abroad, or from public or private research centers.

L'archive ouverte pluridisciplinaire **HAL**, est destinée au dépôt et à la diffusion de documents scientifiques de niveau recherche, publiés ou non, émanant des établissements d'enseignement et de recherche français ou étrangers, des laboratoires publics ou privés.

# First experiments with Cs doped Mo as surface converter for negative hydrogen ion sources.

L. Schiesko<sup>1</sup>, G. Cartry<sup>2</sup>, C. Hopf<sup>1</sup>, T. Höschen<sup>1</sup>, G. Meisl<sup>1</sup>, O. Encke<sup>1</sup>, B. Heinemann<sup>1</sup>, K. Achkasov<sup>2,3</sup>, P. Amsalem<sup>2</sup> and U. Fantz<sup>1</sup>

<sup>1</sup>Max-Planck-Institut für Plasmaphysik, Boltzmannstrasse 2, D-85748 Garching, Germany

<sup>2</sup>Aix Marseille University, CNRS, PIIM, UMR 7345, F-13013 Marseille, France

<sup>3</sup>CEA-Cadarache, IRFM, F-13108 St Paul lez Durance

E-mail: loic.schiesko@ipp.mpg.de

**Abstract.** A study was conducted on the properties of molybdenum implanted with caesium as an approach to reduce the Cs consumption of negative hydrogen ion sources based on evaporated Cs. The depth profiles of the implanted Cs were simulated by SDTrimSP and compared to XPS depth profiling and forward modelling. Good agreement between the measured depth profiles and modelling was found. In particular, one year after implantation, the depth profiles showed no signs of Cs diffusion into the molybdenum, suggesting long term stability of the implanted Cs atoms. The H<sup>-</sup> surface generation mechanisms on the implanted samples in hydrogen plasma and the stability of the H<sup>-</sup> yield during low power hydrogen plasma discharges as long as four hours were investigated. Moreover, an estimation of the work function reduction by the Cs implantation and a comparison of the relative negative ion yields between the implanted samples and highly oriented pyrolytic graphite (HOPG) were performed, leading to the conclusion that the development of Cs doped Mo compounds as surface converter materials should be continued.

## 1. Introduction

The development of negative hydrogen ion sources is an active research topic covering many fields of application, as for example the proton synchrotron booster at CERN [1], neutron therapy [2], spallation neutron sources [3] as well as neutral beam injection (NBI) systems for fusion experiments devices such as LHD [4] or JT60U [5].

Since 2007 the small size (1/8 area of the ITER ion source) RF ion source for negative hydrogen ions [6, 7, 8], developed at IPP Garching, is the ITER baseline design [9]. Currently at IPP, the ELISE [10, 11] test facility (1/2 area of the ITER ion source) is operated to demonstrate the scalability of the small size ion source prototype to larger areas. A full ITER area ion source is currently under construction at Consorzio RFX Padua [12], as well as a complete beam line [13].

Due to its high current drive efficiency ( $0.2 - 0.55 \times 10^{20}$  A/W/m<sup>2</sup>) NBI is also a key candidate as a heating and current drive (H&CD) system for a demonstration fusion power plant (DEMO) [14], in the case of a cw tokamak DEMO scenario for which a high driven current is mandatory.

Negative hydrogen ion sources are based on the conversion of neutral and positive hydrogen ion species ( $H^0 / D^0$  and  $H_x^+ / D_x^+$ ,  $x = 1 \dots 3$ ) into negative ions  $H^- / D^-$  on a converter surface. The negative ion generation yield is greatly enhanced by the evaporation of Cs [15, 16, 17] as it reduces the work function of the surfaces on which it is deposited.

For IPP prototype sources, the source conditioning consists in the careful evaporation of fresh Cs, and typically leads to an increase of the source performance: the extracted negative ion current increases while the amount of co-extracted electrons decreases (see for example [8]). The process of conditioning is delicate: the flux of injected Cs has to be carefully adjusted to maintain the performance of the source. Laboratory experiments confirmed what was empirically guessed when operating prototype sources, i.e. that the high chemical reactivity of the surface deposited Cs layers with background gas components such as oxygen and water (impurities) led to a change of the properties of the Cs layers. Adsorption and absorption of impurities were shown to increase the work function [18]. The passivation of the Cs by the impurities is one of the reasons explaining why high source performance is maintained by continuous evaporation of fresh Cs.

The Cs consumption of the negative hydrogen ion sources is a critical parameter because the maintenance and Cs refilling procedures will strongly depend on it. In contrast to what can be expected by considering the vapour pressure of pure Cs, Cs is not pumped out through the extraction system in negative hydrogen ion sources. A quantitative assessment was performed for both arc-driven and RF ion sources and most of the evaporated Cs was found in the sources with small traces on the grids [19, 20]. As previously mentioned, the need to evaporate fresh Cs in prototype sources is mainly due to the passivation of the already evaporated Cs by impurities [21, 22] but also to the adsorption of Cs to locations which are less accessed by the plasma, leading to a lower redistribution of the Cs in those areas. For IPP prototype sources, the Cs consumption was determined to range between 5 and 10 mg.h<sup>-1</sup> [14].

The first estimate of the ITER NBI Cs consumption was 7 g per half year [23]. The scaling of the Cs consumption to larger source size is arduous and not straightforward. A tentative estimate of the Cs consumption was proposed based on the measurements performed on the now decommissioned IPP's long pulse test facility MANITU: assuming an ITER-like DEMO source (0.2 m<sup>2</sup> extraction area, 60 A extracted current) this leads to 350 - 700 g for a DEMO injector operated 80 % of the year (see [14] for details).

For small (BATMAN, MANITU) and large size (ELISE) IPP sources, the Cs injection systems are based on small amounts (around 1 g) of Cs stored in an oven. The refilling procedure of these ovens is routinely achieved and does not present any particular difficulty. In contrast, for DEMO a much larger storage is needed, as well as the devel-

opment of a refilling procedure during operations which avoid a complete maintenance of the ion source. The Cs consumption of the source should also be the lowest possible to minimize the amount of activated Cs (evaporated Cs and Cs stored in the oven) by the hard neutron radiation coming from the tokamak. Even if the DEMO maintenance period is yet unknown, the removal of the accumulated Cs in the source is a drawback of the use of Cs ion sources.

It then appears clearly, from the different points evoked in the previous paragraphs, that a reduction of the amount of Cs can only be beneficial to operate the negative hydrogen ion sources at high performance.

Alternatives to Cs is currently an active research topic [24, 25, 26, 27, 28]. The main goal is to operate a Cs free negative ion source with a performance at least comparable to the cesiated sources. To this aim one must find or develop a converter surface with a negative hydrogen ion yield comparable to cesiated surfaces currently used in negative ion sources and which has to keep its properties stable for a long time, i.e. real cw operation. Candidates such as lanthanum hexaboride [24, 25], diamond and boron doped diamond (BDD) [26] as well as highly oriented pyrolytic graphite (HOPG) [27, 28] are interesting materials, some of them already showed that one could generate  $H^- / D^-$  ions.

Here it is proposed to study the properties of Mo implanted with Cs as a surface converter material. Mo was chosen as substrate because the converter surface of the NNBI sources (also called plasma grid, PG) are foreseen to be made of copper covered by molybdenum. By implanting Cs into Mo, one expects to modify the surface properties of the Mo in order to have a stable compound with a reduced work function. One of the mile stones of this proposal is to dope the Mo in a way to obtain a material with a work function significantly lower than pure Mo, the ultimate goal being to obtain a material with a stable work function lower or as close as possible to what was measured in laboratory experiments when evaporating Cs on Mo substrates (2.8 eV in vacuum) [24]. If the work function reduction is not sufficient to operate NNBI sources in a Cs free environment, it is expected that working with a PG work function lower than pure Mo will lead to a decrease of the Cs consumption of NNBI sources, which in turn will ease the operations by shortening the conditioning and reconditioning processes. Reducing the Cs needed to operate the sources at high performance promises a higher stability and reproducibility of the extracted currents during long pulses [25] as well as a reduction of the Cs storage size for DEMO-like ion sources. A smaller amount of evaporated Cs in DEMO-like ion sources will also lead to less frequent maintenance and Cs storage refill.

Several studies already showed that Cs implanted into Mo led to a reduction of the work function [29, 30, 31, 32]. In their work Tompa, Carr and Seidl investigated the work function changes by varying the dose and energy (up to 1 keV) of the  $Cs^+$  ions impinging a Mo surface. It was observed that increasing the energy of the  $Cs^+$  ions led

to a decrease of the coverage as the ions become implanted more deeply [29, 30]. Depth profiles were also analytically computed, via a simple model, with and without diffusion of the Cs into the Mo lattice. Sputter profiling showed evidence of diffusion [30, 31]. Interestingly, the maximum decrease of the work function (-2.6 eV) was observed for a surface coverage of 60 % (0.6 mono layers) [29, 30], which is in good agreement with other measurements where the minimum was found between 40 % and 60 % [33]. For low coverage of the surface by Cs, the interaction of Cs atoms with crystalline Mo can be accurately described by density functional theory [34]. The authors show that a dipole effect induced by the interaction of the Cs and Mo atoms reduces the work function and is most effective for a Cs coverage between 40 % and 60 %, corresponding to 0.4 to 0.6 mono layers.

Several properties are nevertheless required in order to use Cs doped Mo compound as surface converter for negative ion sources. Among them, the long term stability (year scale) of the implanted Cs atoms must be proven. The stability and the reproducibility of the extracted currents during long cw hydrogen and deuterium plasmas must be demonstrated. The recovery of the negative ion yield after venting the source is also important.

In this paper, in order to provide a proof of principle for the use of Cs doped Mo compounds as surface converters and to reduce the implantation costs, very small amounts of Cs were implanted in Mo samples in order to obtain a surface Cs atomic fraction lower than 10 % and to constitute a near surface reservoir, the details of which will be given below. The first part of this paper is dedicated to the modeling of the implantation with SDTrimSP in order to determine the energy and dose of Cs required for reaching the requested atomic fractions and the constitution of the near surface reservoir. A comparison of the calculated Cs depth profiles and the experimental ones obtained by XPS-depth profiling a few days and one year after implantation will be shown. The second part is dedicated to the description of the plasma reactor and the experimental results. In particular, the surface negative ion generation mechanisms in hydrogen plasma are identified, and the recovery of the relative negative ion yield after venting the source is discussed. Moreover the stability of the relative  $H^-$  yield during 4 h cw operation is demonstrated and an estimate of the work function reduction induced by the implanted Cs atoms is given. Finally, a comparison of the relative negative ion yield between the implanted samples, pure Mo and HOPG [27, 28, 35] is presented.

## **2. SDTrimSP program, forward modelling and XPS-depth profiling**

In order to achieve a surface Cs concentration lower than 10 % and to obtain a near surface reservoir, the implantation profiles were computed by SDTrimSP [36, 37]. SDTrimSP is based on the static TRIM.SP [38] and the dynamic TRIDYN [39, 40]. SDTrimSP models atomic collisions in amorphous targets to calculate ranges, sputtering and reflexion yields, depth distribution of implanted atoms, as well as energy

distributions of backscattered and sputtered atoms. The binary collision approximation is used to handle the atomic collisions. The trajectories of both incident ions and the recoil atoms are treated as series of collisions. In the static case, the target composition is fixed during the simulation. In the dynamic case, modifications of the composition of the target by ion bombardment are taken into account and the target composition is updated regularly. Diffusion and segregation are not included in the calculations.

Among several combinations of ion doses and energies tested as input parameters for SDTrimSP it was chosen to implant the samples in a two-step sequence and with a very small total dose of  $10^{16} \text{ cm}^{-2}$  caesium atoms: first, a dose of  $5 \cdot 10^{15} \text{ cm}^{-2}$  caesium atoms at 15 keV followed by  $5 \cdot 10^{15} \text{ cm}^{-2}$  at 10 keV.

The choice of a two-step implantation sequence was motivated by the need to build up a near surface reservoir of Cs over several nanometers combined with a fair surface atomic fraction. The beneficial effect that is expected from a near surface reservoir of Cs is to mitigate a decrease of the surface Cs concentration due to diffusion into the bulk. The Cs reservoir is expected to prevent an unwanted slow increase of the work function with time by increasing the near surface available Cs atoms to maintain the work function at a low level for an extended period of time.

To this aim, the first sequence at 15 keV is needed in order to implant the Cs deeply into the samples. However the drawbacks of implanting at 15 keV are a high total sputtering yield leading to a poor surface and bulk Cs atomic fraction. The second sequence at a lower energy of 10 keV permits an increase of the surface and the near surface (2-3 nm below the surface) Cs concentration. The already implanted Cs increases the bulk material stopping power, while the reduction of the implantation energy down to 10 keV decreases both the total (and partial) sputtering yields and the implanted depth. In figure 1a), the depth profiles were both computed by SDTrimSP in dynamical mode for  $5 \cdot 10^{15} \text{ cm}^{-2}$  caesium atoms at 15 keV followed by  $5 \cdot 10^{15} \text{ cm}^{-2}$  caesium atoms at 10 keV with an implantation angle for the ions of  $45^\circ$  and  $50^\circ$  with respect to the normal incidence respectively. The incidence angle of the Cs atoms simulates the roughness of the samples and was treated as a free parameter. It can be thought of as the effective mean value of the microscopic angle with the rough surface.

The samples were made of 99.95 % polycrystalline Mo for a size of  $1 \text{ cm}^2$  and were implanted by an external company according to the dose and energies previously described. The samples temperature was lower than  $100^\circ \text{C}$  during the whole implantation process. In order to have a non-implanted surface state as close as possible to the PG surface roughness, the samples were not polished prior to implantation. Profilometry showed a peak-to-peak surface structure prior to and after implantation of  $0.8 \mu\text{m}$ . No post implantation annealing was performed. After implantation all the samples were maintained in air during five days. Sample 1 was then maintained under ultra high vacuum ( $10^{-10} \text{ mbar}$ ), the other four under primary vacuum ( $10^{-2} \text{ mbar}$ ).

The samples were analyzed by X-ray photoelectron spectroscopy (XPS) depth profiling using a PHI 5600 ESCA system with hemispherical analyzer in the constant analyzer energy mode. Spectra were recorded at a pass energy of 23.5 eV with a step width of

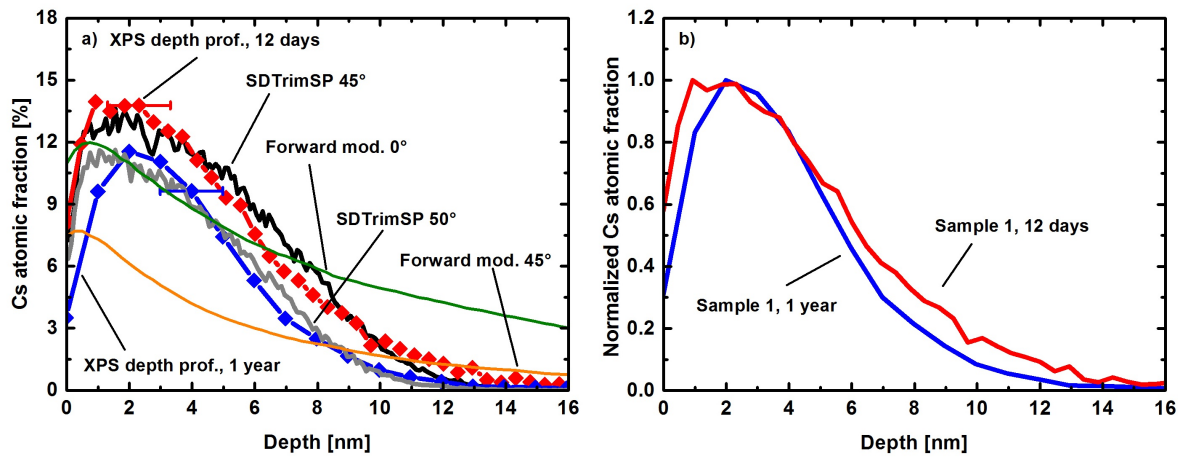


**Figure 1.** a) Caesium atomic fraction for: XPS depth profiling performed twelve days and one year after implantation, the SDTrimSP simulation for  $45^\circ$  and  $50^\circ$  incidence angles, the forward modelling for  $0^\circ$  and  $45^\circ$  incidence angles, b) normalization of the experimental curves of fig 1a).

0.1 eV, using a standard X-ray source with Mg Ka radiation (1253.6 eV). The analysis area was determined by the Omnicfocus lens to a spot with a diameter of  $400 \mu\text{m}$  ( $150 \mu\text{m}$  for the first measurement series). Depth profiling was done by scanning a 10 keV  $\text{Ar}^+$  ion beam over an area sufficiently larger than the measurement spot (Atomica WF 421 Microfocus Ion Gun).

The first part of this study was dedicated to the stability of the implanted Cs with time for samples stored at room temperature (either in air or vacuum), and not exposed to hydrogen plasma.

Figure 1) shows a set of measured and simulated Cs depth profiles. The red and the blue curves with the diamond symbols are measured XPS depth profiles 12 days and one year after implantation at two different locations of the same sample. The sample was stored in air at room temperature during the first twelve days and then in ultra-high vacuum ( $10^{-10}$  mbar) the rest of the time.

For these two curves the measured intensities were converted to a Cs atomic fraction via sensitivity factors and the depth was calculated as product of the sputter yield and the Ar fluence. The surface caesium concentration is of the order of 5% (0.05 monolayer). One can clearly distinguish the Cs reservoir between 1 and roughly 4 nm.

The black and grey curves are the Cs depth profile calculated with SDTrimSP with an implantation angle of  $45^\circ$  and  $50^\circ$  with respect to normal incidence. The depth profiles obtained directly by SDTrimSP are indicative and cannot be directly compared to the experimental results determined by XPS depth profiling, despite the good agreement, because Ar erosion and ion beam mixing induced by the Ar sputtering are not taken into account. For this reason, forward modelling based calculations were performed.

The green and the violet lines on figure 1a also are based on SDTrimSP simulations

but additionally include a forward modelling of the XPS depth profiling process [64]: it consists in using the Cs depth profile from the SDTrimSP implantation simulation as an input for a second SDTrimSP simulation taking into account the Ar erosion process occurring during the XPS depth profiling. The aim is to include the ion beam mixing effect [64] in order to improve the accuracy of the simulated depth profiles. Based on this simulation, one can calculate the resulting XPS intensity ratios from the photoelectron cross-section and the electron inelastic mean free path. Finally, the XPS intensity ratios and the Ar fluence are converted to the Cs atomic fraction and depth, respectively, via the same procedure (i.e. sensitivity factors and sputter yield) as applied to the experimental data.

The comparison of the XPS depth profiling results with the results from forward modelling indicates that the experimental data and the SDTrimSP simulations do not completely agree: the simulation for an implantation angle of  $0^\circ$  is in good agreement with experimental profiles up to 6 nm but is then too large for greater depths. The simulations based on an implantation angle of  $45^\circ$  for the Cs ions gives a better agreement at larger depths, but do not match close to the surface. From this it follows that either the comparison between simulations and measurements is hampered by the roughness of the sample, or that the measured depth profile is different from the one predicted by SDTrimSP because the diffusion of Cs for example is not taken into account in the modelling.

In figure 1a, the difference in magnitude observed between the measurement performed twelve days and one year after implantation seems to be explained by the fact that the samples were not polished and the that the two different locations where the measurements were performed may have different roughness. As XPS depth profiling is a destructive method, two measurements in the same identical spot are not possible. The hypothesis of roughness is supported by the fact that several other depth profiles of this particular sample were performed regularly (results not shown here), the magnitude of the Cs concentration and the shape of the intermediate profiles still being in the range of the results presented in figure 1a. Moreover, diffusion profiles typically show a decrease of the maximum concentration height as well as a broadening of the distribution, which is not the case. The last argument is supported by similar normalized depth profiles presented in figure 1b.

Thus, one can conclude that the implanted Cs is particularly stable for samples stored at room temperature, either in air or vacuum, and not exposed to hydrogen plasma. One can also conclude that surface roughness is the probable reason explaining the discrepancy observed between XPS depth profiling and forward modelling. Polished samples will be used during the next campaign in order to see whether or not a better agreement between experimental and calculated depth profiles can be obtained.

### 3. Experimental setup, results and discussion

#### 3.1. Experimental setup

The plasma experiments were performed with an ECR reactor [41] based on a modified Helicon source and presented in figure 2a. The microwave ECR source is from Boreal Plasma and was operated at 2,45 GHz. A more detailed description of the ECR source can be found in [42]. The reactor is equipped with a quadrupole mass and energy spectrometer (QMS) Hiden EQP 300. The tuning of the QMS was an important aspect of this study. For each sample bias the same tuning of the QMS was used in order to ensure a constant transmission function.

An RF-compensated movable Langmuir probe from STRAATUM was used to determine the electron and positive ion densities, the plasma and floating potentials as well as the electron temperature. The base pressure was  $10^{-7}$  mbar. Typically the discharge parameters were 0.3 Pa hydrogen pressure, 100 W of injected power resulting in a positive ion density (electron density) of  $3 \cdot 10^{14} \text{ m}^{-3}$ , a plasma potential of 6 V, an electron temperature of 0.5 eV and a dissociation degree  $n\text{H}/n\text{H}_2$  of 1 % in the sample vicinity. The plasma composition determined by the QMS showed that it was largely dominated by  $\text{H}_3^+$  with a proportion of 63 % followed by  $\text{H}^+$  with 28 % and by  $\text{H}_2^+$  with 9 %. A thermocouple placed at the back of the sample allowed for sample temperature measurements. The samples can be heated by driving a current in a thermocoax resistor placed behind the sample, and the sample holder can be rotated. Only one implanted sample was used during all the plasma experiments.

Figure 2b) presents the sample and QMS arrangement. Typically, a sample bias ( $V_s$ ) lower than the plasma potential ( $V_p$ ) is applied to the sample while the QMS nozzle is grounded. The positive ions are attracted by the potential difference  $V_0 = (V_{pl} - V_s)$  and strike the sample, while the negative ions created on the surface are repelled by the same potential difference and collected by the QMS where they are analyzed according to their energy. Under this bias configuration, the surface-produced negative ions are self-extracted from the plasma. The plasma potential being higher than the QMS nozzle potential no negative ion generated in the plasma volume can be extracted.

The distance between the mass spectrometer and the sample was 67 mm. Electron stripping ( $e + \text{H}^- \rightarrow 2e + \text{H}$ ) becomes an effective loss mechanism of the negative ions when the electron temperature is below a few eV [43]. It can here be neglected because the electron density was only  $3 \cdot 10^{14} \text{ m}^{-3}$ . The other loss mechanisms such as mutual neutralization ( $\text{H}^- + \text{H}^+ \rightarrow \text{H} + \text{H}$ ) [44, 45], which slightly depends on ion temperature; associative detachment ( $\text{H} + \text{H}^- \rightarrow e + \text{H}_2$ ) [46] and the non-associative detachment ( $\text{H} + \text{H}^- \rightarrow e + \text{H} + \text{H}$ ) [47] both of which depending on the atomic hydrogen temperature can also be neglected [41]. At 0.3 Pa, the mean free path for stripping of a negative ion by collision with  $\text{H}_2$  is also much larger than the QMS - sample distance [41, 48]. One can then conclude that the negative ion losses on their way to the mass spectrometer are negligible.

In the following the surface  $\text{H}^-$  generation mechanisms will be discussed.

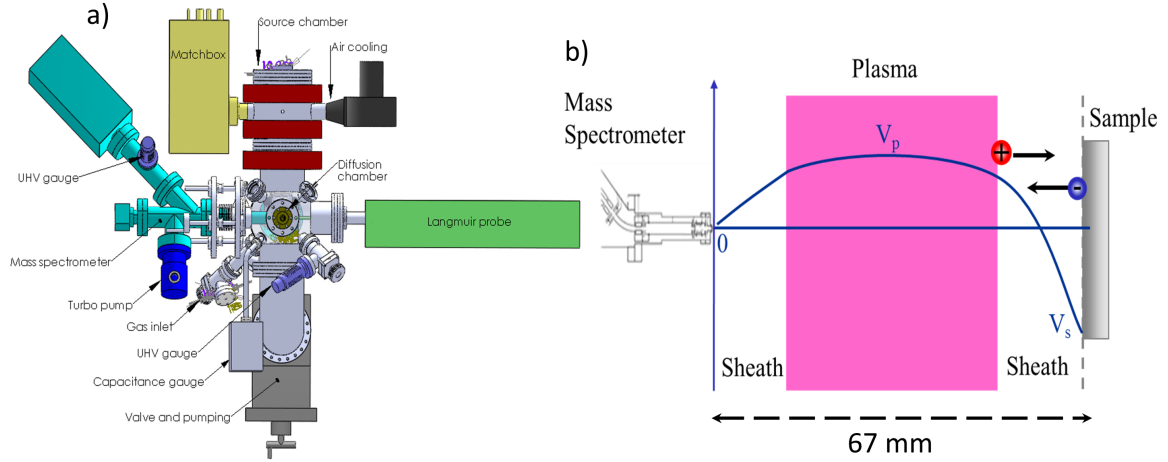


**Figure 2.** a) Sketch of the ECR reactor test bed [41], b) sample-mass spectrometer arrangement,  $V_s$  and  $V_p$  are the sample and plasma potential respectively.

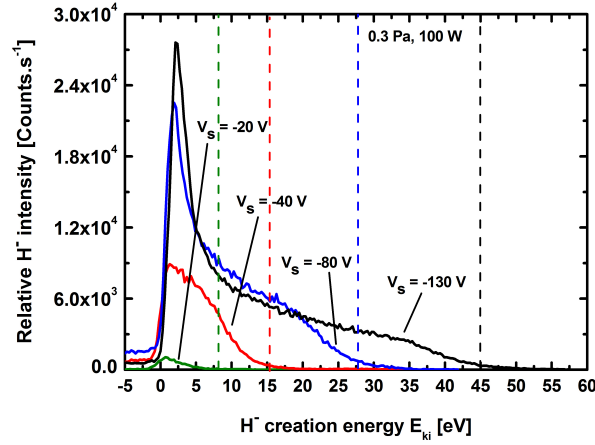


**Figure 3.**  $H^-$  creation energy for a sample bias of -20 V, -40 V, -80 V, -130 V for a 0.3 Pa  $H_2$ , 100 W plasma. The dashed lines correspond to  $E_0/3$  for each sample biases.

### 3.2. Negative ion generation mechanisms

Because of the thermal equilibrium between the positive ions and the neutrals in the plasma, the positive ions  $H_x^+$  ( $x=1...3$ ) strike the sample surface with an energy  $E_0 = e(V_{pl} - V_s)$  and are neutralized upon impact. As described in [41] the mass spectrometer measures the total kinetic energy of the negative ions:

$$E_T = E_{ki} + e(V_{pl} - V_s) - eV_{pl} \quad (1)$$

with  $E_{ki}$  being the energy at which a negative ion was created on the surface. On the right-hand side, the second term of eq. (1) is the energy difference between the sample and plasma potentials leading to an acceleration directed toward the QMS for the surface

created negative ions, the third term acting as a deceleration for the negative ions due to the QMS nozzle being grounded (see figure 2b for a sketch of the potentials). For a constant sample bias, all the surface created negative ions will experience the same

$$E_r = e(V_{pl} - V_s) - eV_{pl} \quad (2)$$

As a consequence, the key parameter to determine the surface generation mechanisms is the surface creation energy  $E_{ki}$ .

Two  $H^-$  surface generation mechanisms are expected [27, 28, 35, 49]: the backscattering of a positive ion ( $H_x^+$ ,  $x = 1...3$ ) or a neutral  $H^0$  as  $H^-$  and the sputtering of an adsorbed hydrogen as a negative ion by an incident positive ion.

These two surface mechanisms are also expected as  $H^-$  surface generation mechanisms in NNBI prototype sources. For NNBI prototype sources, most of the negative ions are generated by low temperature neutrals  $H^0$ , the energy of the positive ions hitting the PG is around 1 eV [50]. As a consequence, the energy of the positive ions and neutrals hitting the PG is way below the sputtering energy threshold. Thus, in NNBI prototype sources, the backscattering is probably the dominant surface negative ion generation mechanism.

Let us first consider the backscattering mechanism for a proton that loses no energy when interacting with the surface. The proton will be accelerated toward the surface by the sheath potential drop and thus will gain  $E_0$ . After being neutralized by resonant electron capture prior to collision and then having captured a second electron the resulting  $H^-$  will be repelled from the surface. In this particular case where we assumed an "elastic" backscattering on the surface  $E_{ki}$  is equal to  $E_0$  and is the maximum energy for a negative ion created from a proton. Because the proton is neutralized prior to collision, the described mechanism of the backscattering as  $H^-$  for a proton is in any point similar for a  $H^0$  coming from the bulk plasma and backscattered as a  $H^-$ . The only differences are that  $H^0$  atoms are not accelerated by the sheath potential drop and, being already neutral, capture only one electron.

Molecular ions are dissociated upon impact on the surface, the total kinetic energy of the ion being evenly splitted between the fragments. Assuming again an elastic backscattering, the maximum creation energy of a negative ion coming from  $H_2^+$  and  $H_3^+$  ion will be  $E_2 = E_0/2$  and  $E_3 = E_0/3$  respectively.

The second mechanism is the sputtering of an adsorbed hydrogen as a negative ion by an incident positive ion. SDTrimSP simulations were run to determine the outgoing energy of the H sputtered by the positive ions. Some approximations had to be done: the plasma being mainly made of  $H_3^+$  which is dissociated upon impact, the energy of the impinging ions for each sample bias was then  $E_0/3$  and their mass 1 a.m.u. It was found that the most probable energy (peak) of the sputtered H was around 6 eV for a sample bias of -130 V (43 eV positive ion energy), 4 eV for a sample bias of -80 V (27 eV positive ion energy) and that for lower bias voltages the positive ion energy was below the sputtering threshold.

It then appears from the previous considerations that energy at which the negative ions are created on the surface depend on the generation mechanism.

The experimental results will be discussed in the following section.

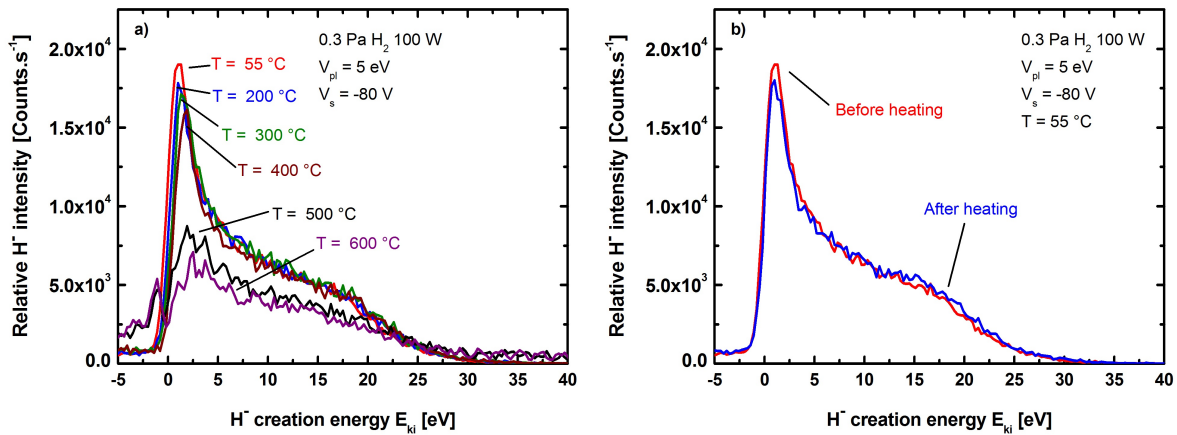
### *3.3. Results and discussion*

Figure 3 shows the measured relative intensity of the  $H^-$  as a function of the creation energy  $E_{ki}$  for sample biases down to -130 V.

Let us first consider the backscattering mechanism. For a sample bias of -80 V and -130 V one observes a main low energy peak followed by a high energy tail. The shape of the negative ion distribution functions are similar to the ones observed on HOPG [28, 35]. The main peak is not present at lower sample biases which will be discussed below. Because the plasma composition is dominated by  $H_3^+$ , the dashed line corresponds to  $E_0/3$  for each sample bias and was plotted to show that the high energy part of the distribution function is the contribution of the backscattering mechanism. One clearly observes in figure 3 that whatever the sample bias, the kinetic energy of the surface created negative ions almost vanishes after  $E_0/3$ , the small extension of the distribution function beyond  $E_0/3$  being attributed to  $H^-$  created from  $H^+$  and  $H_2^+$ . For sample biases equal to -40 V and -20 V one observes a reduction of the number of collected negative ions and a diminution of the height of the main peak. This is related to the sheath voltage drop and to the angular emission of the negative ions (results not presented here [51]): for a sample bias of -80 V or -130 V the negative ions see their trajectories modified by the large sheath voltage drop (in comparison to their creation energy). The negative ions leave the surface in a direction normal to the surface and can be collected by the 150  $\mu\text{m}$  QMS nozzle hole. This is particularly true for low  $E_{ki}$  negative ions. When the sample bias is reduced, then less negative ions leave in normal direction, explaining the decrease of the signal for lower sample biases.

Let us now consider the sputtering mechanism. As discussed in the previous subsection, because the most probable energy of the sputtered hydrogen atoms is a few eV whatever the sample bias is, it seems possible to identify the low energy main peak observed for sample biases lower or equal to -80 V in figure 3 as being due to the sputtering of adsorbed hydrogen as  $H^-$  by the impinging positive ions. Moreover, the fact that no main peak can clearly be distinguished for  $V_s$  equal to -20 V and -40 V in figure 3 is in good agreement with the sputtering calculations showing that the threshold energy is not reached for such small  $V_s$ .

Nevertheless, in order to clearly show that the low energy peak is mainly due to sputtering, the sample was slowly heated up to 600 °C while  $V_s$  was maintained at -80 V with a 0.3 Pa, 100 W plasma. Figure 4a presents the obtained  $H^-$  creation energy for different intermediate temperatures, the reference room temperature measurement



**Figure 4.** a):  $H^-$  creation energy for a sample temperature of  $55^\circ\text{C}$ ,  $200^\circ\text{C}$ ,  $300^\circ\text{C}$ ,  $400^\circ\text{C}$ ,  $500^\circ\text{C}$ ,  $600^\circ\text{C}$  and for a  $0.3\text{ Pa H}_2$ ,  $100\text{ W}$  plasma and  $-80\text{ V}$  sample bias, b):  $H^-$  creation energy for a sample temperature of  $55^\circ\text{C}$  obtained before heating and after cooling phase.

being the spectrum at  $55^\circ\text{C}$  in figure 4a). One observes in figure 4a) that up to  $400^\circ\text{C}$ , the height of the main peak slowly diminishes with temperature while the high energy parts ( $E_{ki} > 7\text{ eV}$ ) still superimpose. At  $500^\circ\text{C}$  and beyond the main peak signal has collapsed while one observes a decrease of the high energy part, the  $H^-$  signals still superimposing for  $E_{ki} \geq 20\text{ eV}$ . The slight decrease of the main peak for temperatures up to  $400^\circ\text{C}$  can be attributed to the decrease of the H surface coverage when the temperature is increased, as already observed in [35] for HOPG.

Several studies examined the retention of hydrogen and deuterium in Mo [52, 53, 54, 55, 56]. It appears from these studies that the onset release temperature of hydrogen isotopes from Mo ranges from  $0^\circ\text{C}$  to  $700^\circ\text{C}$ , the differences being due to the sample temperature during hydrogen implantation and the fluence. Concerning the results presented in this study, it is clear that some hydrogen is implanted into the Mo when the sample is negatively biased, the fluence being anyway smaller than the ones used in [52, 53, 54, 55, 56]. It is then likely that the collapse of the  $H^-$  peak for sample temperatures larger than  $400^\circ\text{C}$  is due to the release of the adsorbed and trapped H when the desorption temperature is reached. Thus, the contribution of the low energy peak is mostly due to the sputtering process. In figure 4a, the remaining signal observed beyond  $400^\circ\text{C}$  can be attributed to the backscattering process because of the disappearance of most of the adsorbed hydrogen and the continuity of the  $H^-$  signal over the full  $E_{ki}$  range. As suggested in [57], the release of hydrogen may not only influence the sputtering yield but also the (negative) ionization efficiency due to the change of the electronic properties of the material in contact with the plasma. This could then explain the decrease of the relative backscattering yield observed for sample temperatures beyond  $400^\circ\text{C}$ .

Moreover, in figure 4a, one can conclude from the unmodified high energy part of the distribution function that:

- the  $H^-$  backscattering yield is not temperature dependent up to  $400^\circ\text{C}$ ,

- up to 400 °C the backscattering mechanism is not dependent on the H surface coverage, as observed in a similar fashion on HOPG [28, 35]. It seems very probable that the backscattering mechanism, among several parameters, mostly depends on the work function.

More importantly, one also observes that up to 400 °C, no particular cleaning effect of the impurities such as water, oxygen etc... is activated by increasing the surface temperature. Indeed, a temperature induced cleaning of the surface would probably lead to a decrease of the work function, and thus to an increase of the relative backscattering  $H^-$  yield which is not observed in figure 4a (the relative sputtering yield should also increase, but the concomitant decrease of the hydrogen coverage would make it difficult to deconvolute). Additionally, the disappearance of the main peak also suggests that the contribution of the neutral  $H^0$  to the relative negative ion yield is small for two reasons: first, the dissociation degree in the source is of the order of 1% and, second, the neutrals have  $0.026 < E_{ki} < 1.12$  eV (half of the Franck-Condon energy). Consequently, one should observe at this energy the contribution of the neutrals to the  $H^-$  yield on the distribution function whatever the sample temperature, which is not the case.

A question nevertheless arises from the results presented in figure 4a. Indeed, the decrease in the relative negative ion yield corresponding to the contribution of the backscattering mechanism observed for  $E_{ki} \geq 7$  eV beyond 400 °C in figure 4a) could also be due to the diffusion of the Cs inside and outside the sample, leading to an increase of the work function. Figure 4b compares the  $H^-$  distribution functions obtained before heating the sample and after the cooling phase, both obtained during the same plasma shot and same sample bias. One can conclude from figure 4b), that the reappearance of the main low energy peak observed on the spectrum after cooling confirms that the sputtering is the dominant low energy generation mechanism because the sample surface is again saturated by atomic hydrogen. More importantly, one can conclude that if Cs diffused because of the increased sample temperature, the variation of the depth profile and more importantly, the variation of the surface Cs concentration was small enough not to noticeably change the work function. This is confirmed by figure 5) where one can see that in comparison to the reference sample (kept at room temperature and never exposed to the plasma), the depth profile of the sample heated and exposed to the plasma shows a lower maximum concentration and a broadening of the Cs distribution, which can be expected in cases of Cs diffusion. The diffusion of the Cs into the Mo sample is however marginal, and the surface Cs atomic fraction is almost identical to the reference sample, which is the probable reason of the stability of the relative  $H^-$  yield prior to and after the sample heating. The result presented in figure 5) is also a hint suggesting the usefulness of implementing a near surface Cs reservoir to mitigate a decrease of the surface Cs atomic fraction.

The recovery of the negative ion yield was tested by recording the relative negative ion yield after having the vessel vented and for a sample maintained at room temperature. No evolution of the  $H^-$  yield could be observed from the start of the plasma after a

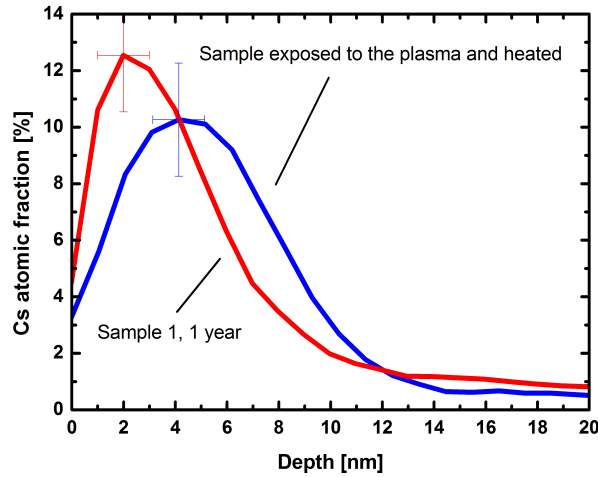


**Figure 5.** Comparison of the depth profiles from the sample 1 (never exposed to the plasma) and the sample used during the plasma campaign.

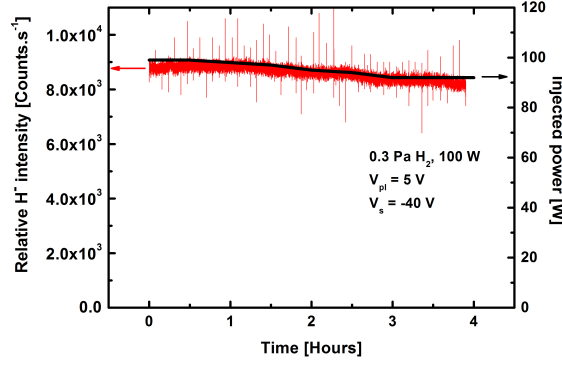
good vacuum was achieved, meaning that the plasma cleaning of the impurities such as oxygen, water etc... adsorbed on the surface was quick. This fact is also supported by the results presented in figure 4a), which does not suggest any cleaning effect when the temperature is raised.

From the previous high temperature results, it seems to be obvious that the long term diffusion of the implanted Cs atoms with high temperature samples and in particular the expected mitigation of the Cs diffusion offered by the near surface reservoir has to be further investigated.

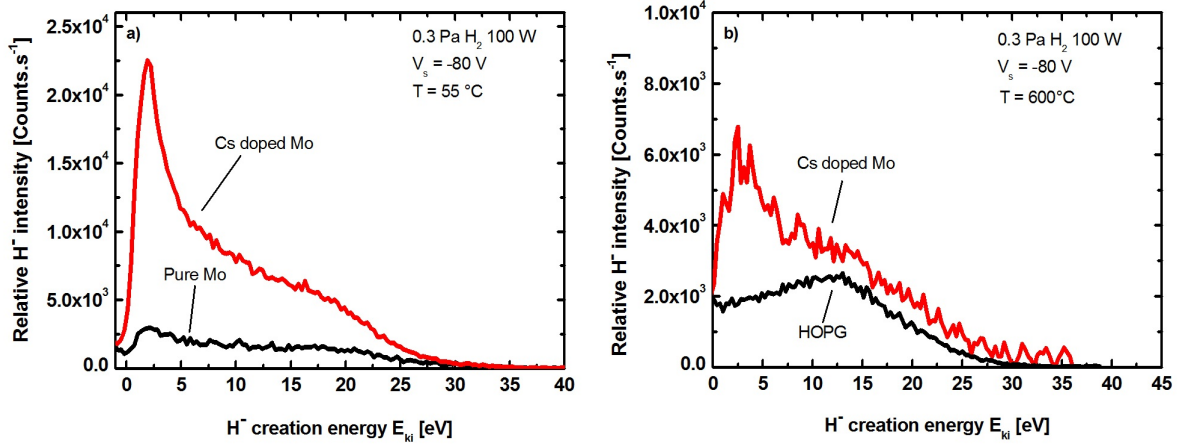
The stability of the relative  $H^-$  yield during long cw plasma pulses is a critical aspect of this study. To this aim, the mass spectrometer was tuned to follow the height of the main peak during a 1 h 30 (not shown here) and 4 h plasma discharge. The plasma parameters and sample bias were kept constant for the full duration in both cases.

Figure 6) presents the variation of the height of the main peak for a plasma pulse of 4h at 0.3 Pa, 100 W of injected power and  $V_s = -40$  V. The sample temperature did not increase during the four hours. The slight decrease of the  $H^-$  signal (-10%) occurring after one hour is due to an observed decrease of the injected power also shown in Figure 6) because of an increase of the reflected power. This small change in the matching is probably due to the warming up of the power supply, the RF transmission line and the matching box. Besides that, one can see in figure 6) that the relative ion yield is particularly stable over long pulse operations.

Figure 7a) compares of the relative negative ion yield between a Cs doped Mo sample and a pure Mo sample both manufactured from the same raw material. The plasma parameters and sample bias were comparable and the mass spectrometer tuning rigorously identical for both cases in order to maintain the same transmission function. One



**Figure 6.** Variation of the relative negative ion yield and of the injected power during 4 h operation.



**Figure 7.** a): comparison of the relative  $H^-$  yield of a Cs implanted sample to pure Mo sample, b): comparison of the relative  $H^-$  yield of a Cs implanted sample to an HOPG sample.

observes clearly that even for around 5% Cs surface proportion, the relative negative ion yield of the Cs doped sample is much larger than the pure Mo sample.

It is known that the formation probability  $P^-$  to create negative ions on metals [58, 59] (and references therein) is given by:

$$P^- \propto e^{-(\phi-A)/\epsilon_n} \quad (3)$$

with  $\phi$  being the work function,  $A$  the electron affinity and  $\epsilon_n$  a parameter whose magnitude should fall in the range 0.5-1 eV and is thought to be dependent on the normal component of the ion velocity [60]. Experimental data [61, 62] however showed that the parameter  $\epsilon_n$  was largely independent of the ion velocity and in the range of 0.2-0.4 eV.

Thus, based on the work function of pure Mo (4.6 eV), it is possible to give a rough estimate of the work function change induced by the implantation of Cs. By defining

$I_{Mo} = \int_0^\infty f_{Mo}(E) dE$  and  $I_{Cs/Mo} = \int_0^\infty f_{Cs/Mo}(E) dE$  the integrals of the  $H^-$  distribution functions in figure 7a) of the pure Mo and Cs doped Mo respectively, as well as  $R = \frac{I_{Cs/Mo}}{I_{Mo}}$  it follows:

$$\frac{I_{Cs/Mo}}{I_{Mo}} = \frac{e^{-(\phi_{Cs/Mo}-A)/\epsilon_n}}{e^{-(\phi_{Mo}-A)/\epsilon_n}} \quad (4)$$

and then

$$\Phi_{Cs/Mo} = \Phi_{Mo} - \epsilon_n \ln(R) \quad (5)$$

with  $\Phi_{Cs/Mo}$  and  $\Phi_{Mo}$  the work functions of the implanted probe and pure Mo respectively. The estimated work function  $\Phi_{Cs/Mo}$  of the Cs doped Mo samples is then comprised between 3.8 for  $\epsilon_n = 0.4$  and 4.2 for  $\epsilon_n = 0.2$  which corresponds to a work function reduction comprised between -0.8 and -0.4 eV. This result is in good agreement with other experiments [58, 59, 63]. One can see that for only 0.05 monolayers of Cs, the reduction of the work function is already non negligible. The work function of the Cs doped Mo samples will be measured in the future in order to confirm the previous estimate.

Figure 7b) compares the relative  $H^-$  ion yield of a Cs implanted sample to an HOPG sample. Again, precautions were taken in order to have very close plasma parameters, same sample temperature and an identical QMS tuning for both samples.

As previously mentioned, in NNBI prototype sources, the backscattering is probably the dominant surface generation mechanism. It was previously shown that at high temperature, most of the negative ions were generated from the backscattering mechanism (see [28, 35] for HOPG). For this reason, figure 7b) compares the relative yields at 600 °C, temperature for which most of the surface generated negative ions were created via the backscattering mechanism, which is mostly dependant of the work function.

One can clearly see in figure 7b) that the negative ion yield of the HOPG is lower than the one observed for Cs-implanted samples, which make Cs doped Mo an interesting candidate.

Future experiments will focus on increasing the surface Cs atomic fraction, to measure the work function and check the stability of the implanted Cs atoms to hydrogen plasmas with a much larger plasma flux. From this study it clearly appears that the Cs diffusion is triggered by the sample temperature. Forthcoming studies will also focus on determining the sample temperature which triggers the Cs diffusion. Another interesting study to perform is also to compare the negative ion yield between Cs doped Mo samples and pure Mo samples covered by evaporated Cs.

In this work the plasma flux was much lower than what can be expected in a prototype source such as BATMAN. Forthcoming experiments will focus on the stability of the depth profiles of probes exposed to hydrogen plasmas with a much larger flux of positive ions. Moreover, plasma experiments and stability measurements will be performed on

samples implanted in a way leading to larger surface and bulk Cs concentrations, the implantation procedure being calculated by SDTrim.SP.

#### **4. Conclusion**

In this paper, Mo samples were implanted by a very small dose of Cs leading to a surface Cs atomic fraction of roughly 5%, which corresponds to 0.05 monolayers. The goal was to test as a proof of principle the stability and material properties of this compound as an efficient surface converter to generate negative hydrogen ions. XPS depth profiling was performed regularly, showing a long term stability proved up to one year. The use of SDTrim.SP allowed the calculation of the implanted depth profiles, whose results were in good agreement with the experimental profiles. The surface generation mechanisms were identified, similarly to a previous work on HOPG: the backscattering of the positive ions as negative ions was found to be the mechanism which gives rise to the high energy part of the negative ion creation energy function, while most of the low energy created negative ions are issued from the sputtering as  $H^-$  of an adsorbed H onto the surface. Temperature measurements permitted to show that Cs could diffuse into and probably outside of the Mo. Increasing the sample temperature did not show an increase of the  $H^-$  ion yield, meaning that no particular cleaning effect of the surface was occurring. Low surface temperature operation is to be preferred, to avoid the Cs diffusion. The recovery of the negative ion yield after venting was checked and the stability of the  $H^-$  yield in plasma was confirmed several times and up to 4 h continuous operation. By comparing the relative yields of the Cs doped samples and pure Mo samples it was possible to give an estimate of the work function of the implanted sample which ranges between 3.8 and 4.2 eV (4.6 eV for pure Mo). Finally a comparison with HOPG showed that the implanted samples had a larger yield.

#### **5. Acknowledgments**

The authors would like to thank Dr. P. Franzen for fruitful discussions. This project has received funding from the European Unions Horizon 2020 research and innovation programme under grant agreement number 633053. The views and opinions expressed herein do not necessarily reflect those of the European Commission.

#### **6. References**

- [1] Lettry J. et al., Rev. Sci. Inst. 85, (2014) 02B122.
- [2] Schmidt J. S., Koubek B., Schempp A., Tan C. Y., Bollinger D. S. et al., Phys. Rev. ST Accel. Beams 17, (2014) 030102
- [3] Stockli M. P., Ewald K. D., Han B. X., Murray S. N. Jr. et al., Rev. Sci. Inst. 85, (2014) 02B137
- [4] Takeiri Y. et al., Nucl. Fusion 46, (2006) S199210
- [5] Kojima A. et al., Nucl. Fusion 51, (2011) 083049
- [6] Speth E. et al., Nucl. Fus. 46 (2006) 220.

- [7] Franzen P. et al., Nucl. Fus. 47 (2007) 264.
- [8] Schiesko L. et al., Plas. Phys. & Cont. Fus. 53 (2011) 085029.
- [9] Hemsworth R., Tanga A. and Antoni V., Rev. Sci. Inst. 79, (2008) 02C109.
- [10] Fantz U. et al., Rev. Sci. Inst. 85, (2014) 02B305.
- [11] Bonomo F. et al., Plas. Phys. & Cont. Fus. 56 (2014) 015006.
- [12] P. Sonato et al., Fusion Eng. Des. 84, (2009) 269.
- [13] Chitarin G. et al., Rev. Sci. Instrum. 83 (2012) 02B107.
- [14] Franzen P. and Fantz U., Fus. Eng. & Design 89, (2014) 2594.
- [15] Belchenko Yu. I., Dimov G. I., and Dudnikov V. G., Nucl. Fus. 14 (1974) 113-114.
- [16] Belchenko Yu. I., Dimov G. I., and Dudnikov V. G., Proc. Symp. Production and Neutralization of Negative Hydrogen Ions and Beams, Brookhaven, 1977 (BNL, Upton, NY, 1977).
- [17] Belchenko Yu. I., Rev. Sci. Instrum. 64 (1993) 1385.
- [18] Gutser R., Wimmer C. and Fantz U., Rev. Sci. Instrum. 82, (2011) 023506.
- [19] Boilson D., Ellingboe A., Faulkner R., Hemsworth R., de Esch H., Krylov A. et al., Fus. Eng. Design 74 (2005) 295298.
- [20] Krylov A., Boilson D., Fantz U., Hemsworth R., Provitina O., Pontremoli S. et al., Nucl. Fus. 46 (2006).
- [21] Fantz U., Gutser R. and Wimmer C., Rev. Sci. Instrum. 81, (2010) 02B102.
- [22] Fantz U. and Wimmer C., Rev. Sci. Instrum. 83, (2011) 02B110.
- [23] Okumura Y., Fujiwara Y., Kashiwagi M., Kitagawa T. and K. Miyamoto, Rev. Sci. Instrum. 71, (2000) 1219.
- [24] Fantz U., Gutser R. and Wimmer C., Rev. Scientific Instrum. 81 (2010) 02B102.
- [25] Fantz U. and Wimmer C., Rev. Scientific Instrum. 83 (2011) 02B110.
- [26] Kumar P., Ahmad A., Pardanaud C. et al., J. Phys. D: Appl. Phys. 44 (2011) 372002.
- [27] Schiesko L. et al., Plasma Sources Sci. Technol. 17 (2008) 035023.
- [28] Schiesko L., Carrère M., Layet J.-M. and Cartry G., Applied Phys. Lett. 95, (2009) 191502.
- [29] Tompa G. S. et al., App. Phys. Lett 48, (1986) 1048.
- [30] Carr W. et al., Journ. Vac. Sci. Tech. A 5, (1987) 1250.
- [31] Tompa G. S. et al., Surf. Sci., 198, (1988) 431.
- [32] Isakhanov Z. et al. Tech. Phys. 56, (2011) 546.
- [33] Soukassian P. et al., Solid State Comm. 44, (1982) 1375.
- [34] Chubb S. R. et al., Phys. Rev. B. 36, (1987) 4112.
- [35] Schiesko L., Carrère M., Layet J.-M. and Cartry G., Plasma Sources Sci. Technol. 19, (2010) 045016.
- [36] Eckstein W. *Computer Simulation of Ion Solid Interactions, Springer Series in Materials Science*, 10, Springer, Berlin (1991).
- [37] Eckstein W. et al., IPP Rep. 12/3, Max-Planck-Institut für Plasmaphysik, Garching (2007).
- [38] Biersack J. P. and Eckstein W., App. Phys. A 34, (1984) 73.
- [39] Möller W. and Eckstein W., Nucl. Inst. Meth. B 2, (1984) 814.
- [40] Möller W., Eckstein W. and Biersack J. P., Comput. Phys. Comm. 51, (1988) 355.
- [41] Ahmad A., Dubois J., Pasquet T., Carrère M., Layet J.-M., Faure J.-B., Cartry G., Kumar P., Mina T., Mochalsky T. and Simonin A., Plasma Sources Sci. Technol. 22 (2013) 025006.
- [42] Béchu S., Soum-Claude A., Bès A., Lacoste A., Svarnas P., Aleiferis S., Ivanov A. A. and Bacal M., Phys. Plasmas 20 (2013) 101601.
- [43] Takayanagi K. and Suzuki H., Cross Sections for Atomic Processes, Vol. 1 (Institute of Plasma Physics, Nagoya University, Nagoya, Japan, 1978).
- [44] Szucs S., Karemera K., Terao M. et al., J. Phys. B 17, (1984) 1613.
- [45] Peart B., Bennett M. A. and Dolder K., J. Phys. B 18, (1985) L439.
- [46] Poulaert G., Brouillard F., Claeys W. et al., J. Phys. B 11, (1978) L671.
- [47] Janev R. K., Langer W. D., Evans K., and Post D., Elementary Processes in Hydrogen-Helium Plasmas (Springer-Verlag, Berlin- Heidelberg, 1985).

- [48] Phelps A.V., J. Phys. Chem. Ref. Data 19 (1990) 653.
- [49] Cartry G. et al., Phys. Plasmas 19 (2012) 063503.
- [50] Wunderlich D., Schiesko L. et al., Plasma Phys. Control. Fusion 54, (2012) 125002.
- [51] Schiesko L., Cartry G. et al., To be published.
- [52] Haasz A.A. and Davis J. W., Journ. Nucl. Mat. 241-243, (1997) 1076.
- [53] Tanabe T., Hachino H. and Takeo M., Journ. Nucl. Mat. 176-177, (1990) 666.
- [54] Sakamoto R., Muroga T. and Yoshida N., Journ. Nucl. Mat. 233-237, (1996) 776.
- [55] Van Veen A. and Filius H. A., Journ. Nucl. Mat. 155-157, (1988) 1113.
- [56] Causey R. A., Kunz C. L. and Cowgil D. F., Journ. Nucl. Mat. 337-339, (2005) 600-603.
- [57] Ahmad A., Pardanaud C., Carrère M., Layet J.-M., Gicquel A., Kumar P., Eon D., Jaoul C., Engeln R. and Cartry G., J. Phys. Appl. Phys. 47, (2014) 085201
- [58] Gnaser H., Phys. Rev. B 54 (1986) 16456.
- [59] Kudriavtsev Y., Asomoza R., Appl. Surf. Sci. 167 (2000) 12.
- [60] Lang N. D., Phys. Rev. B 27, (1983) 2019.
- [61] Yu M. L., Phys. Rev. Lett 40, (1978) 574.
- [62] Yu M. L., Phys. Rev. B 26, (1982) 4731.
- [63] Swanson L. W. and Strayer R. W., J. Chem. Phys. 48, (1968) 2421.
- [64] Meisl G et al., New J. Phys. 16, (2014) 093018.